

# PCCP

Accepted Manuscript



This is an *Accepted Manuscript*, which has been through the Royal Society of Chemistry peer review process and has been accepted for publication.

*Accepted Manuscripts* are published online shortly after acceptance, before technical editing, formatting and proof reading. Using this free service, authors can make their results available to the community, in citable form, before we publish the edited article. We will replace this *Accepted Manuscript* with the edited and formatted *Advance Article* as soon as it is available.

You can find more information about *Accepted Manuscripts* in the [Information for Authors](#).

Please note that technical editing may introduce minor changes to the text and/or graphics, which may alter content. The journal's standard [Terms & Conditions](#) and the [Ethical guidelines](#) still apply. In no event shall the Royal Society of Chemistry be held responsible for any errors or omissions in this *Accepted Manuscript* or any consequences arising from the use of any information it contains.



PCCP

PAPER

## STM investigation of structural isomers: alkyl chain position induced self-assembly at liquid/solid interface

Yi Hu, Kai Miao, Bao Zha, Li Xu\*, Xinrui Miao and Wenli Deng\*

Received 00th January 20xx,  
Accepted 00th January 20xx

DOI: 10.1039/x0xx00000x

www.rsc.org/

Investigating and regulating the self-assembly structure is of great importance in 2D crystal engineering and it is also gaining significant interest in surface studies. In this work, we systematically explored the variation of self-assembled patterns induced by the changeable side chain position. Moreover, molecules with different alkyl chain length ( $n = 15, 16$ ) were also synthesized and probed for the purpose of understanding how odd/even number of carbon atoms in the peripheral chains can affect the molecular adlayers. Structural isomers of bis-substituted anthraquinone derivatives 1,8-A-2OC<sub>n</sub>, 2,6-A-2OC<sub>n</sub>, 1,4-A-2OC<sub>n</sub> and 1,5-A-2OC<sub>n</sub> ( $n = 15, 16$ ) were used and investigated by STM. 1,8-A-2OC<sub>16</sub> and 1,8-A-2OC<sub>15</sub> molecules adopted Z-like I and Linear I structures, respectively. 2,6-A-2OC<sub>16</sub> and 2,6-A-2OC<sub>15</sub> molecules were severally arranged in Linear II and Linear III configurations. 1,4-A-2OC<sub>n</sub> ( $n = 15, 16$ ) molecules were staggered in a Z-like II fashion and 1,5-A-2OC<sub>n</sub> ( $n = 15, 16$ ) molecules displayed a Linear IV nanostructure. Therefore, we make a conclusion that self-assembly structures of anthraquinone isomers are chain-position-dependent and designing isomeric compounds can be taken into consideration on regulating assembled structures. Besides, 2D nanopatterns of 1,8-A-2OC<sub>n</sub> and 2,6-A-2OC<sub>n</sub> can be regulated by odd/even property of the side chains, but this is not the case for 1,4-A-2OC<sub>n</sub> and 1,5-A-2OC<sub>n</sub>, ascribing to the difference of driving forces for them. It is believed that the results are of significance to the fields of alkyl chain position induced assembly configurations and surface researches of structural isomers.

### 1. Introduction

Molecular self-assembly is a ubiquitous phenomenon in nature and has been recognized as a powerful mean of fabricating functional nanomaterials.<sup>1</sup> Thus, designing and creating two-dimensional (2D) architectures on solid surfaces based on molecular self-assembly are appealing great attention at present.  $\pi$ -Conjugated system can be achieved by employing well-designed molecules as building blocks<sup>2,3</sup> and it has promoted advances in the field of organic materials, for example, molecular devices, molecular-scale electronics and liquid crystal materials.<sup>4,5</sup> Therefore, understanding the organism of molecules on substrate is fundamental for development of molecular nanostructures and nanodevices.<sup>2,6-15</sup> Scanning tunneling microscopy (STM) is a preferred technique for the investigation of self-assembled monolayers under ultrahigh vacuum conditions, liquid/solid or air/solid interface.<sup>16,17</sup> STM offers submolecular visualization and also manipulation of the adsorbates. Successful formation and the subsequent visualization of the adlayer require balance between various forces.<sup>18</sup> In general, with the purpose of successfully controlling 2D molecular arrangements, the following noncovalent interactions and experimental parameters need to be considered. i) Optimization of intermolecular interactions, for

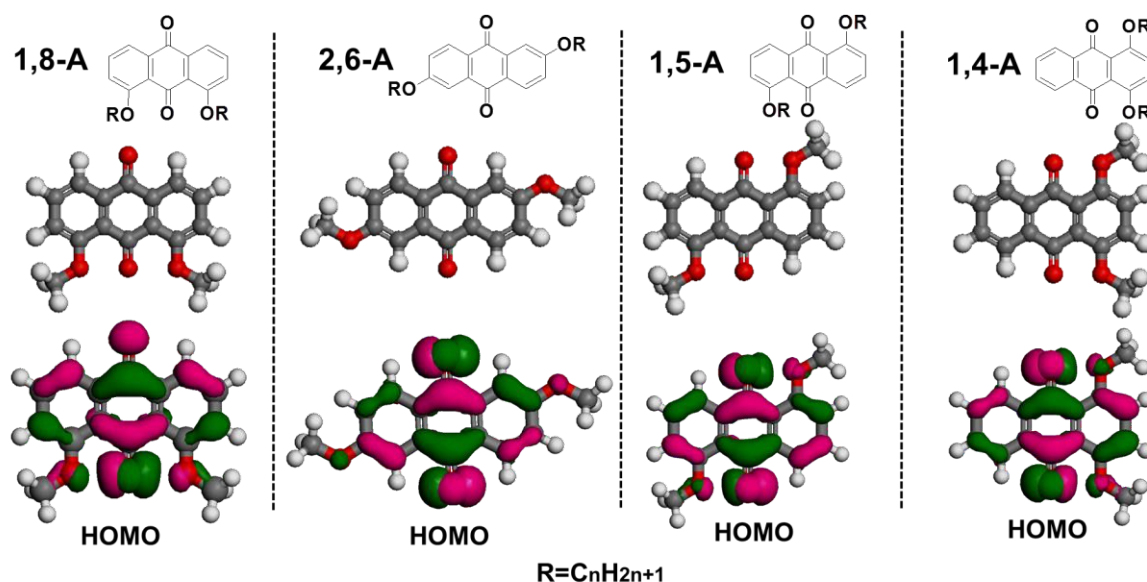
instance, hydrogen bonds<sup>19-21</sup>, metal-ligand coordination<sup>22-24</sup>, dipolar coupling<sup>25-28</sup>, and van der Waals interactions<sup>29</sup>. ii) Molecule–substrate interactions. Molecules adsorb on the surface typically *via* van der Waals interaction, which can be modulated by functional groups and change of the substrate.<sup>30</sup> iii) Experimental conditions. Temperature<sup>31-34</sup>, concentration of the solution<sup>20,35-38</sup>, timing of scanning<sup>39</sup> are well-known to play an important role on 2D network formation.

Chemical structure, among other crucial factors which determine self-assembled nanopatterns, is of ever increasing importance in 2D crystal engineering. Structural isomers are common in organic chemistry. They are a series of molecules, which have the same molecular formulas, but different constitutional formulas. Disaffinity in chemical structure can result in completely different chemical and physical properties, such as color, appearance, melting behavior, steric configuration, photoelectric performance and so on. With the development in preparing supramolecular assemblies, designing and synthesizing structural isomers have attracted lots of attention.<sup>40,41</sup> A large number of papers have reported the effect of odd/even number of carbon atoms in substituent alkyl chains on molecular structures.<sup>42-46</sup> This is a usual phenomenon in many systems, ascribing to the demand of minimizing steric repulsion between the methyl groups, and it is a suggestion that the formation of 2D nanostructure is dominated by the interactions between alkyl chains.<sup>44</sup>

Different self-assembly structures from isomers of tetrathienoanthracene derivatives have been reported by Fu *et al.*<sup>41</sup> They showed that a slight geometric difference between the two

College of Materials Science and Engineering, South China University of Technology, Guangzhou 510640, China. E-mail: mslxu@scut.edu.cn, wldeng@scut.edu.cn; Tel: 86-20-22236708

† Electronic Supplementary Information (ESI) available: Detailed description of experimental section and additional STM images. See DOI: 10.1039/x0xx00000x



**Fig. 1** Chemical structures, molecular models, and the calculated HOMO orbitals (alkyl chains are replaced by methyl substituents for ease of calculation) of 1,8-A, 2,6-A, 1,5-A, 1,4-A derivatives.

isomers (position of the sulfur atoms) may lead to dramatic change in 2D molecular networks. Yoshihiro and coworkers reported various 2D structures of bipyridine derivatives.<sup>40</sup> Structural isomers of *p*-substituted ( $1C_{16p}$ ) and *m*-substituted ( $1C_{16m}$ ) bipyridine with hexadecyl adopted completely different assembly structures. Namely,  $1C_{16p}$  showed almost linear form of zigzag-type alignment of the  $\pi$ -conjugated units, whereas,  $1C_{16m}$  adopted Z-shaped morphology *via* alkyl chain interdigitation. Anthraquinone derivatives have been explored in the field of liquid crystal because of their low cost, high temperature stability, and ambient condition stability.<sup>47</sup> Matthew and his group reported self-assembly properties of 1,5-di(octyloxy)-anthraquinone (15DA) on highly ordered pyrolytic graphite (HOPG).<sup>48</sup> 15DA formed well-ordered monolayers though octyl chain interdigitation and planar adsorption of the anthracene ring. Yanhu *et al.* demonstrated dipolar controlled self-assembly of anthracene derivatives.<sup>27</sup> 1,5-Bis-substituted-anthracene with odd carbon atoms in the alkyl chain formed linear structures with the anthracene groups in adjacent rows pointing to the same direction, whereas, that with even carbon atoms adopted reverse direction of the anthracene moieties. As such, subtleties of the self-assembly can be explored systematically with an emphasis on the role of molecular structure and odd–even effect.

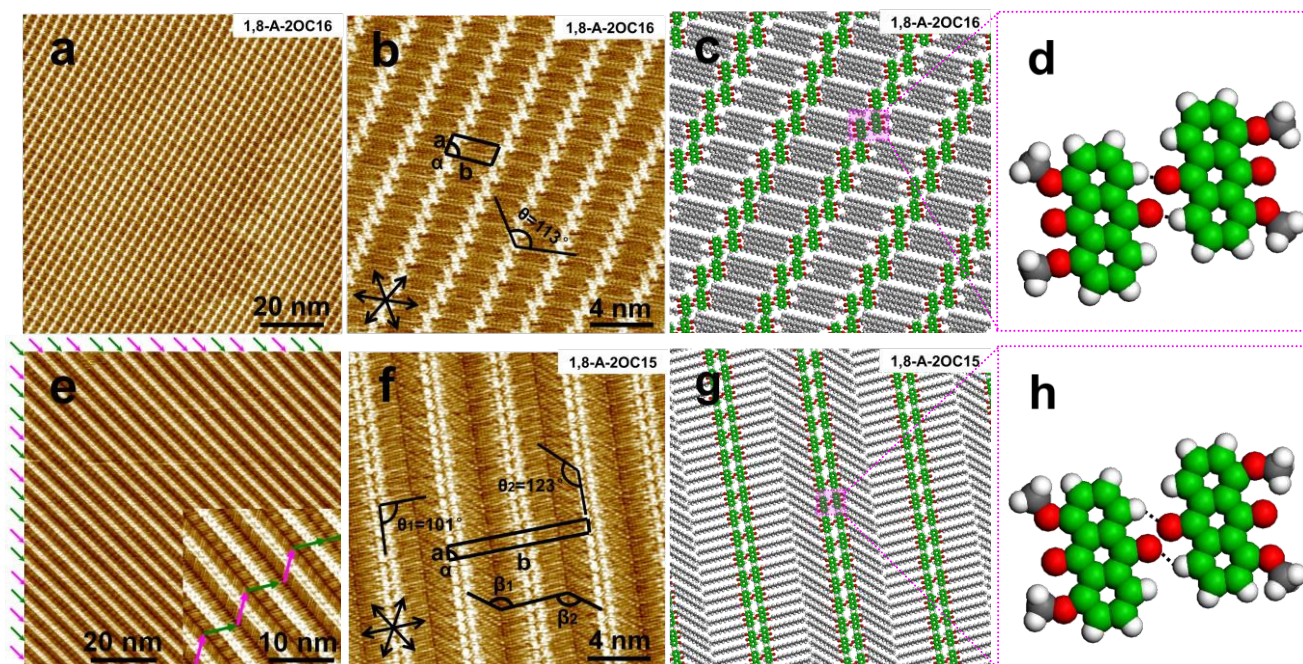
Herein, we explored different 2D nanopatterns which were obtained because of structural changes with STM at the liquid/solid interface. There are four kinds of anthraquinone isomers, which consist of an anthraquinone unit and two side chains in 1,8-position, 2,6-position, 1,4-position and 1,5-position: 1,8-bis(*n*-alkoxy)-9,10-anthracenedione (1,8-A), 2,6-bis(*n*-alkoxy)-9,10-anthracenedione (2,6-A), 1,4-bis(*n*-alkoxy)-9,10-anthracenedione (1,4-A) and 1,5-bis(*n*-alkoxy)-9,10-anthracenedione (1,5-A), as shown in Fig. 1. For the purpose of exploring how odd/even number of carbon atoms in the side chains can influence the self-assembled networks, we synthesized tetradecyl and pentadecyl substituted anthraquinone derivatives, respectively. The relative position of the substituted side-chains leads to a number of molecular configurations and

entirely different physical and chemical properties. In this paper, we primarily probed the structural isomerism induced 2D self-assembled feature and mechanism and incidentally studied their differential scanning calorimetry (DSC) performance and ultraviolet (UV) absorption spectrum.

## 2. Experimental Section

Structural isomers of 1,8-A, 2,6-A, 1,4-A and 1,5-A were synthesized as described in the supporting information (Scheme S1<sup>†</sup>), and then recrystallized repeatedly in order to ensure the purity. The solutions of the products dissolving in  $CH_2Cl_2$  were prepared for observation of their colors (Fig. S1<sup>†</sup>). 1-Octanoic acid was purchased from Tokyo Chemical Industry and used without further purification. The molecules were dissolved in 1-octanoic acid. The solutions used in our STM work were under a concentration of 50% saturation and the values are given in the corresponding sections. At first, 100% saturated solutions were prepared, and then they were diluted to 50% saturated according to accurate proportion. The samples were prepared by depositing a droplet (about  $1\mu L$ ) of solution on a freshly cleaved atomically flat surface of HOPG (quality ZYB, Bruker, USA). STM experiments were performed on a Nanoscope IIIa Multimode SPM (Bruker, USA) under ambient condition (temperature: 15–20°C, humidity: 50%). The tips were mechanically cut from Pt/In wires (80/20). All images were recorded with constant current mode and shown without further processing. Imaging conditions are given in the corresponding figure captions. Material studio 4.4 was used to build molecular models of the assembled structures and to calculate the HOMO orbitals. The DSC experiments were conducted with a scan rate of  $10\text{ }^\circ C\text{ min}^{-1}$  for heating and cooling traces (instrument information: NETZSCH DSC 200F3). The UV absorption spectrums were tested by dissolving the compounds in  $CH_2Cl_2$  (the concentrations are given in the corresponding sections) using ultraviolet spectrometer (equipment: Agilent Cary 60).





**Fig. 2** (a) Large-scale and (b) high-resolution STM images of 1,8-A-2OC<sub>16</sub> self-assembled monolayer on HOPG surface. Concentration:  $3.92 \times 10^{-3}$  M. (c) Molecular model of the Z-like structure (Z-like I). (e) Large-scale STM image of 1,8-A-2OC<sub>15</sub> self-assembled monolayer on HOPG surface (Linear I). The pink and green arrows represent different alkyl chain orientations of the tail-to-tail stripes. Concentration:  $4.84 \times 10^{-3}$  M. (f) High-resolution STM image of 1,8-A-2OC<sub>15</sub>. (g) Molecular model of the lamellar structure. A set of black arrows in (b) and (f) show the basic symmetry axis of the graphite substrate. The angles between the alkyl chain and the macroaxis of the anthraquinone unit in (b) and (f) are marked by the value of  $\vartheta$ ,  $\vartheta_1$ ,  $\vartheta_2$ . Weak hydrogen bonds C=O...H-C forming 2D architectures are illustrated in (d) and (h). The long alkyl chains are replaced by methyl groups. Imaging conditions:  $I_t = 550$  pA,  $V_{\text{bias}} = 700$  mV for (a) and (b),  $I_t = 580$  pA,  $V_{\text{bias}} = 790$  mV for (e) and (f).

### 3. Results

Self-assembly patterns were immediately observed by STM measurement after depositing a drop of solution onto the HOPG surface. 1-Octanoic acid was selected as the solvent, and no solvent coadsorption was observed. Therefore, we conclude that the structural isomers of anthraquinone derivatives adopted configurations which are as denser as possible, with the solvent exerting its role only as a dispersant.

#### 3.1 Self-assembly of 1,8-A-2OC<sub>n</sub> ( $n = 15, 16$ )

Initially, we investigated the self-assembled structures that were obtained by dropping 1,8-A-2OC<sub>16</sub> solution at the 1-octanoic acid/HOPG interface. Large-scale STM image of 1,8-A-2OC<sub>16</sub> self-assembled adlayer is shown in Fig. 2a. It can be clearly seen that bright stripes and dark troughs form the ordered pattern without any defects. The bright stripes are ascribed to the  $\pi$ -conjugated units of 1,8-A-2OC<sub>16</sub>, while the dark troughs are the peripheral alkyl chains. Fig. 2b is a high-resolution STM image, which reveals the arrangement details of this Z-like structure, named as Z-like I. The black solid arrows depicted in the left bottom of Fig. 2b displays the main symmetry axes of the graphite under the monolayer. Every two 1,8-A-2OC<sub>16</sub> molecules take arrangement in a head-to-head fashion and then all of the acetabuliform dimers aggregate with each other, forming Z-like stripes. Alkyl chains in adjacent stripes are interdigitated and extending along the direction of the basic

graphite axis. Therefore, van der Waals interactions of molecule–molecule and molecule–substrate are maximally enlarged, resulting in a stable and closely-packed 2D self-assembled monolayer. The angle between the side chain and the macroaxis of the anthraquinone unit is measured to be  $\vartheta = 113 \pm 2^\circ$  (as shown in Fig. 2b). A structural model is tentatively proposed in Fig. 2c, which is in accordance with the high-resolution STM image. According to the periodicity of the molecular self-organization, a unit cell is superimposed in Fig. 2b. The lattice constants are determined to be  $a = 1.2 \pm 0.3$  nm,  $b = 2.3 \pm 0.3$  nm and  $\alpha = 75 \pm 1^\circ$ . Every unit cell consists of two molecules and the calculated area density is  $1.33$  nm<sup>2</sup> per molecule.

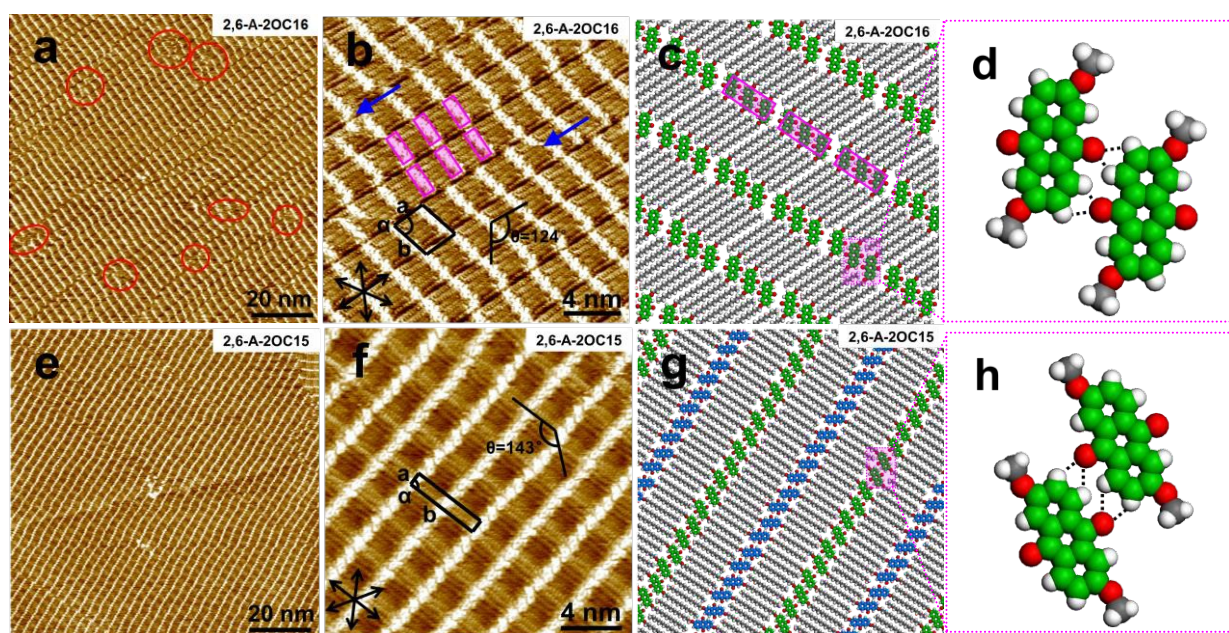
With the decreasing of the alkyl chain length by one carbon atom, different assembled structure was discerned. As shown in Fig. 2e, the large-scale STM image reveals that 1,8-A-2OC<sub>15</sub> adopted linear configuration, defined as Linear I. The emergence of bright stripes and dark troughs are ascribed to high and low tunneling current of the  $\pi$ -conjugated anthraquinone units and alkyl chains. Fig. 2f is the high-resolution STM image, showing the detailed packing pattern of this linear configuration. It is obvious that the alkyl chains are arranged in a tail-to-tail fashion, instead of interdigitated ones as in the case of 1,8-A-2OC<sub>16</sub>. We have experimentally proved that this tail-to-tail fashion is not concentration-dependent. The pink and green arrows in Fig. 2e represent different orientation of the side-chains. Nevertheless, the arrangements of the orientation along which the chains extend are



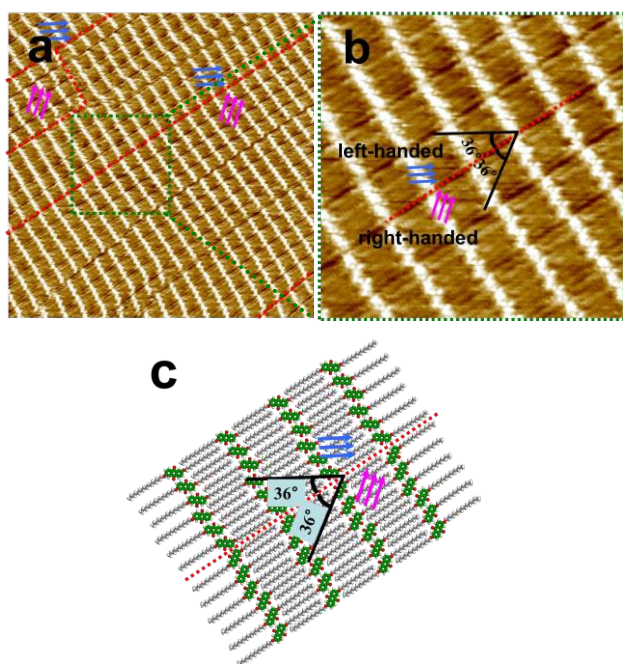
irregular and random, means, the tail-to-tail alkyl chains of 1,8-A-2OC<sub>15</sub> molecules in adjacent rows are arranged in either parallel or V-like fashions. The black solid arrows in Fig. 2f demonstrate the 3-fold symmetry of HOPG substrate. An STM image consists of the 1,8-A-2OC<sub>15</sub> molecules and the HOPG surface can be observed by varying the tunneling bias (see supporting information, Fig. S2†), and this image is a powerful evidence that alkyl chains extend along the main orientation of the graphite lattice. The angle  $\beta_1$  and  $\beta_2$  in Fig. 2f are measured to be  $120 \pm 1^\circ$ , which allow the skeletons of the alkyl chains to match with the graphite lattice. This is proved to be one of the driving force for the formation of stable self-assembled adlayer in 2D engineering system.<sup>46</sup> The angles between the orientation of the alkyl chains and the anthraquinone moieties are measured to be  $\vartheta_1 = 101 \pm 1^\circ$ ,  $\vartheta_2 = 123 \pm 1^\circ$ . On the basis of molecular arrangement, a structural model for the ordered linear monolayer is proposed in Fig. 2g. A unit cell is outlined in Fig. 2f and the parameters are determined to be  $a = 0.8 \pm 0.2$  nm,  $b = 8.8 \pm 0.2$  nm and  $\alpha = 89 \pm 2^\circ$ . Every unit cell consists of four molecules and the calculated area density is  $1.78$  nm<sup>2</sup> per molecule. The 1,8-A-2OC<sub>n</sub> ( $n = 15, 16$ ) adlayers are formed *via* van der Waals interactions between the  $\pi$ -conjugated backbones, as also between the adsorbates and substrate. In addition, hydrogen bonds make great contribution to stabilizing the Z-like and linear structures, as the enlarged pictures shown in Fig. 2d and 2h. In this work, hydrogen bonds are formed with the carbonyl groups acting its role as an acceptor and hydrogen atoms in its neighboring anthraquinone as a donor.

### 3.2 Self-assembly of 2,6-A-2OC<sub>n</sub> ( $n = 15, 16$ )

Fig. 3a shows a typical large-scale STM image of the 2,6-A-2OC<sub>16</sub> adlayer physisorbed at liquid/solid interface of HOPG. The structural details are resolved by a high-resolution STM image shown in Fig. 3b. The angle between the alkyl chain and the macroaxis of the anthraquinone is measured to be  $\vartheta = 124 \pm 2^\circ$ . It can be clearly seen that the basic unit of the monolayer is a number of trimers, which are indicated by pink rectangles. Interestingly, we found that no matter how the domains change, molecules tend to gather consistently, every three together except for some accidental circumstance, means single molecule missing or dislocation (indicated by blue arrows in Fig. 3b), which are rarely to be observed. Molecules in a trimer gather together *via* van der Waals interactions and C=O...H-C hydrogen bonds (Fig. 3d) between the  $\pi$ -conjugated anthraquinone units, and then all of the alkyl chains in adjacent rows interdigitate with each other, forming this stable 2D arrangement (named as Linear II). However, molecules within a molecular row do not form perfectly straight lines. Periodic molecular dislocation along the direction of the alkyl chains can be explained on the basis of strong molecule-substrate interactions and registry mechanism of the side chains with the underlying graphite.<sup>1</sup> Careful observation suggests that the liquid/solid surface is covered by lots of small domains, instead of highly ordered monolayer, and as a consequence, structural defects are a common phenomenon, as denoted by red circles in Fig. 3a. This may be a



**Fig. 3** (a) Large-scale STM image of 2,6-A-2OC<sub>16</sub> self-assembled monolayer on HOPG surface. Structural defects are denoted by red circles. Concentration:  $2.79 \times 10^{-4}$  M. (b) High-resolution STM images of 2,6-A-2OC<sub>16</sub> molecules. Six pink rectangles represent the trimers which make up the basic unit of the adlayer. Structural defects (single molecule dislocation or missing) are indicated by blue arrows. (c) Molecular model of the trimer linear structure (Linear II). (e) Large-scale and (f) high-resolution STM images of 2,6-A-2OC<sub>15</sub> self-assembled monolayer on HOPG surface. Concentration:  $1.98 \times 10^{-4}$  M. (g) Molecular model of the lamellar structure (Linear III). A set of black arrows in (b) and (f) show the basic symmetry axis of the graphite substrate. The angles between the alkyl chain and the macroaxis of the anthraquinone unit in (b) and (f) are marked by the value of  $\vartheta$ . Weak hydrogen bonds C=O...H-C forming 2D architectures are illustrated in (d) and (h). The long alkyl chains are replaced by methyl groups. Imaging conditions:  $I_t = 570$  pA,  $V_{\text{bias}} = 820$  mV for (a) and (b),  $I_t = 610$  pA,  $V_{\text{bias}} = 870$  mV for (e) and (f).



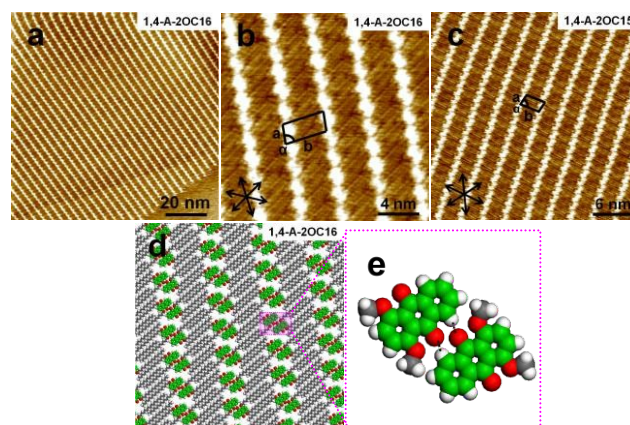
**Fig. 4** (a) STM images of chiral monolayer of the 2,6-A-2OC<sub>16</sub>, with a small area enlarged in (b). Concentration:  $2.79 \times 10^{-4}$  M. (c) Chiral structure model based on the molecular arrangement. Imaging conditions:  $I_t = 570$  pA,  $V_{\text{bias}} = 820$  mV.

proof that trimers in this monolayer show mobility along the direction of the main graphite axis. A unit cell is outlined in Fig. 3b and the parameters are determined to be  $a = 2.3 \pm 0.5$  nm,  $b = 2.6 \pm 0.5$  nm and  $\alpha = 77 \pm 2^\circ$ . Every unit cell consists of three molecules and the calculated area density is  $1.94$  nm<sup>2</sup> per molecule. Fig. 3c is the temporary molecular model and it is in good agreement with the STM results.

To gain further insight into exploring how odd/even number of carbon atoms in the side chains can affect the self-assembly structures, another compound, 2,6-A-2OC<sub>15</sub> was also synthesized and investigated by STM measurement. 2,6-A-2OC<sub>15</sub> molecules adopt linear structure (named as Linear III), as shown in the large-scale STM image of Fig. 3e. The monolayer which covers the HOPG surface with orderly domains is constituted from stripes. The high-resolution STM image in Fig. 3f manifests more structural details. Anthraquinone units in adjacent rows are not parallel, but rather forming a V-like fashion. This rotation of a whole row is needed for the matching of neighboring carbon atoms in adjacent stripes, then alkyl chains are fully interdigitated, and thus minimize the steric repulsion.<sup>43,45</sup> This V-like fashion is an indication that one of the driving forces for this kind of assembled configuration is interactions between the alkyl chains. The angle between the side chain and the macroaxis of the anthraquinone is measured to be  $\vartheta = 143 \pm 1^\circ$ . A unit cell is superimposed in Fig. 3f. The unit cell parameters are determined to be  $a = 0.9 \pm 0.3$  nm,  $b = 4.7 \pm 0.3$  nm and  $\alpha = 85 \pm 1^\circ$ . Every unit cell consists of two molecules and the calculated area density is  $2.11$  nm<sup>2</sup> per molecule. On the basis of a large amount of high-resolution STM images, a structural model for this molecular structure is proposed in Fig. 3g (the rotated rows are depicted with blue carbon atom skeletons), which is in good

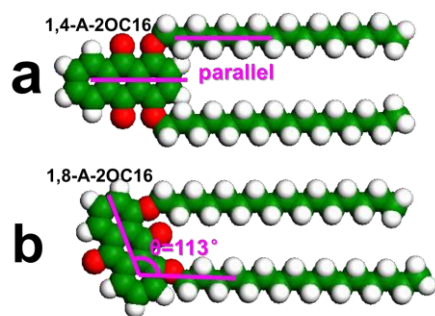
consistent with the experimental results. Hydrogen bond between adjacent anthraquinone units, as shown in Fig. 3h, is another kind of the main interactions to force molecules to arrange in this linear fashion.

Moreover, chirality is a common phenomenon which is observed during our STM performance. 2D chirality of molecular self-assembly on solid surface has attracted lots of attention.<sup>49</sup> In this study, chirality was observed as shown in Fig. 4. Several domains with the anthraquinone moieties orienting to different direction can be clearly recognized, as marked by blue (left-handed) and pink (right-handed) arrows. A small area is enlarged in Fig. 4b. The two enantiomeric domains are separated by red dotted lines, and their anthraquinone units form an angle of  $72^\circ$  ( $36^\circ + 36^\circ$ ). The chiral domains are mirror symmetry and cannot be superimposed by rotating of any angle. Interestingly, alkyl chains on two sides of the red dotted line are parallel to each other, assuming that they are extending in a comfort way, without inter-collisions and unstable domain boundaries. A proposed molecular model for this chiral structure is depicted in Fig. 4c. Achiral molecule of 2,6-A-2OC<sub>16</sub> self-assembled into chiral structures on achiral surface of HOPG. Similar chiral phenomenon has been explored and explained by reduced freedom and constraint of the substrate lattice.<sup>50-53</sup> Statistical analysis of more than ten images (scanning area:  $100 \times 100$  nm<sup>2</sup>) collected at different locations from different samples reveal that the emergence probability of left-handed and right-handed structures is almost 1:1. The calculated average coverage ratios are 47.2% for left-handed network and 52.8% for right-handed pattern. We guess that the two enantiomorphous configurations are regardless of priorities and the coverage ratios for them would furtherly approach 50% if the collected large-scale images are as more as possible.



**Fig. 5** (a) Large-scale and (b) high-resolution STM images of 1,4-A-2OC<sub>16</sub> self-assembled monolayer on HOPG surface. Concentration:  $4.98 \times 10^{-3}$  M. A set of black arrows in (b) show the basic symmetry axis of the graphite substrate. (c) Self-assembly pattern of 1,4-A-2OC<sub>15</sub>. Concentration:  $5.34 \times 10^{-3}$  M. (d) Molecular model of the zigzag structure (Z-like II) based on the STM image of 1,4-A-2OC<sub>16</sub>. (e) Illustration of C=O...H-C hydrogen bonding interactions within the dimer aggregations. The long alkyl chains are replaced by methyl groups. Imaging conditions:  $I_t = 590$  pA,  $V_{\text{bias}} = 860$  mV for (a) and (b),  $I_t = 640$  pA,  $V_{\text{bias}} = 830$  mV for (c).





**Fig. 6** Molecular models of 1,4-A-2OC<sub>16</sub> (a) and 1,8-A-2OC<sub>16</sub> (b). (a) Alkyl chains in the 1-position and 4-position spin to the same side, parallel to the macroaxis of the anthraquinone unit. (b) Side chains in the 1-position and 8-position are on the same side of the  $\pi$ -conjugated anthraquinone moiety.

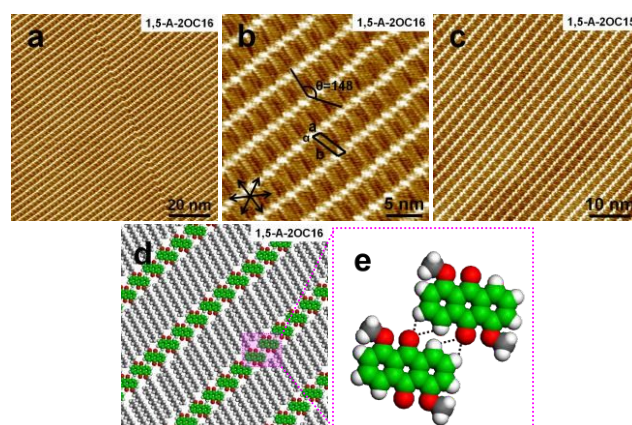
### 3.3 Self-assembly of 1,4-A-2OC<sub>n</sub> ( $n = 15, 16$ )

Alkyl chain position provides an excellent approach on controlling 2D self-assembly ordering. 1,4-A-2OC<sub>n</sub> ( $n = 15, 16$ ) were used here, as another compound of anthraquinone isomers. Fig. 5a is the large-scale STM image of 1,4-A-2OC<sub>16</sub> physisorbed on HOPG surface. A zigzag structure defined as Z-like II can be discerned. The high-resolution image, as shown in Fig. 5b, displays the arrangement details. Every two molecules gather together in a head-to-head fashion, forming an acetabuliform dimer. This is very familiar with the assembly patterns of 1,8-A-2OC<sub>16</sub> (Fig. 2b). Careful observation suggests that alkyl chains in the 1-position and 4-position spin to the same side, parallel to the macroaxis of the anthraquinone unit, as indicated in Fig. 6a. However, side chains of 1,8-A-2OC<sub>16</sub> are on the same side of the  $\pi$ -conjugated anthraquinone moieties, and they can form closely packed arrangement without spin of the peripheral alkyl groups, as shown in Fig. 6b. This is a powerful evidence that ether groups show great flexibility during the self-assembly process and as a consequence, alkyl chains adopt appropriate rotation in consideration of closest packing and minimizing adsorption energy. A unit cell consists two molecules is overlaid with the measured parameters of  $a = 1.4 \pm 0.4$  nm,  $b = 3.5 \pm 0.4$  nm and  $\alpha = 86 \pm 2^\circ$ . The calculated area density is  $2.44$  nm<sup>2</sup> per molecule. Fig. 5d is the proposed structural model for the Z-like II arrangement and it is in good agreement with the STM results. C=O $\cdots$ H-C hydrogen bonds between the  $\pi$ -conjugated anthraquinone units are the main forces in the acetabuliform dimers, as shown in Fig. 5e. In addition, 1,4-A-2OC<sub>15</sub> molecules were investigated and we found that there are no differences on structural patterns between 1,4-A-2OC<sub>16</sub> and 1,4-A-2OC<sub>15</sub> molecules, whether in large-scale STM images (Fig. S3a<sup>†</sup>) or in high-resolution ones (Fig. 5c and S3b<sup>†</sup>). Structural model, unit cell parameters and hydrogen bonds for 1,4-A-2OC<sub>15</sub> are shown in Fig. S3 (ESI<sup>†</sup>). Therefore, we conclude that odd/even property of alkyl chains show no impact on structural diversity of 1,4-A-OC<sub>n</sub> ( $n=15, 16$ ) and the driving forces for the self-assembly process are molecule–molecule, molecule–substrate and hydrogen bonding interactions.

### 3.4 Self-assembly of 1,5-A-2OC<sub>n</sub> ( $n = 15, 16$ )

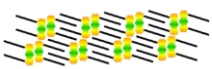
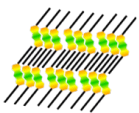

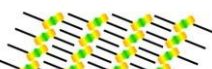
1,5-A-2OC<sub>n</sub> ( $n = 15, 16$ ) molecules showed great central symmetry and they self-assembled on the graphite surface into identical

structures no matter number of the carbon atoms in the peripheral alkyl chain is odd or even. Fig. 7a is the large-scale STM image of 1,5-A-2OC<sub>16</sub>. The HOPG substrate is covered by orderly arranged molecules with their side chains fully extended and interdigitated. This lamella structure is named as Linear IV. Details of the assembled pattern are demonstrated in Fig. 7b. A set of black arrows are imposed in the left bottom, as an indication of the symmetry axis of the graphite lattice. The HOPG surface has a pronounced influence on the configuration of molecules, as the alkyl chains are running parallel to one of the main substrate axes. The angle between the alkyl chain and the macroaxis of the anthraquinone group is measured to be  $\vartheta = 148 \pm 2^\circ$ . A unit cell is outlined in Fig. 7b and the parameters are determined to be  $a = 1.0 \pm 0.1$  nm,  $b = 3.1 \pm 0.1$  nm and  $\alpha = 83 \pm 1^\circ$ . Every unit cell consists of one molecule and the calculated area density is  $3.08$  nm<sup>2</sup> per molecule. Fig. 7d is the temporary molecular model for 1,5-A-2OC<sub>16</sub> and it is in good agreement with the STM results. This model can also be used to illustrate the molecular structure of 1,5-A-2OC<sub>15</sub>, which has been shown in the large-scale STM image of Fig. 7c. Further investigation provided detailed information of this linear structure is shown in Fig. S4 (ESI<sup>†</sup>). Alkyl chains of 1,5-A-2OC<sub>15</sub> form an angle of  $\vartheta = 117 \pm 2^\circ$  with the macroaxis of the anthraquinones (Fig. S4b<sup>†</sup>). Area density is calculated to be  $2.97$  nm<sup>2</sup> per molecule. In addition, careful observation suggests that molecules in the monolayer are closely packed, without  $\pi$ -conjugated anthraquinone spinning to form V-like fashion, as in the case of 2,6-A-2OC<sub>15</sub>. This can also be regarded as an indication that the driving forces for this lamella structure of 1,5-A-2OC<sub>n</sub> ( $n = 15, 16$ ) are van der Waals interactions between molecule–molecule, molecule–substrate, and hydrogen bonds among anthraquinone moieties (Fig. 7e and S4d<sup>†</sup>).



**Fig. 7** (a) Large-scale and (b) high-resolution STM images of 1,5-A-2OC<sub>16</sub> self-assembled monolayer on HOPG surface. Concentration:  $2.87 \times 10^{-3}$  M. A set of black arrows in (b) show the basic symmetry axis of the graphite substrate. (c) Self-assembly pattern of 1,5-A-2OC<sub>15</sub>. Concentration:  $1.96 \times 10^{-3}$  M. (d) Molecular model of the linear structure (Linear IV) based on the STM image of 1,5-A-2OC<sub>16</sub>. (e) Illustration of C=O $\cdots$ H-C hydrogen bonding interactions within the linear structure. The long alkyl chains are replaced by methyl groups. Imaging conditions:  $I_t = 530$  pA,  $V_{\text{bias}} = 750$  mV for (a) and (b),  $I_t = 600$  pA,  $V_{\text{bias}} = 820$  mV for (c).

**Table 1.** Comparison of 1,8-A, 2,6-A, 1,4-A and 1,5-A ( $n = 15, 16$ ) polymorphs by molecular modelling

Molecule	Structural model	phase	basic unit	$a$ (nm)	$b$ (nm)	$\alpha$ ( $^\circ$ )	$\vartheta$ ( $^\circ$ )	$N^a$	$S$ (nm $^2$ ) $^b$
1,8-A		Z-like I	dimer	$1.2 \pm 0.3$	$2.3 \pm 0.3$	$75 \pm 1$	$113 \pm 2$	2	1.33
				$0.8 \pm 0.2$	$8.8 \pm 0.2$	$89 \pm 2$	$\frac{123 \pm 1}{101 \pm 1}$	4	1.78
2,6-A		Linear II	trimer	$2.3 \pm 0.5$	$2.6 \pm 0.5$	$77 \pm 2$	$124 \pm 2$	3	1.94
				$0.9 \pm 0.3$	$4.7 \pm 0.3$	$85 \pm 1$	$143 \pm 1$	2	2.11
1,4-A		Z-like II	dimer	$1.4 \pm 0.4$	$3.5 \pm 0.4$	$86 \pm 2$	0	2	2.44
				$1.5 \pm 0.1$	$3.5 \pm 0.1$	$74 \pm 1$	0	2	2.52
1,5-A		Linear IV	single molecule	$1.0 \pm 0.1$	$3.1 \pm 0.1$	$83 \pm 1$	$148 \pm 2$	1	3.08
				$1.1 \pm 0.2$	$2.7 \pm 0.2$	$88 \pm 2$	$117 \pm 1$	1	2.97

$^a N$  = number of molecules per unit cell.  $^b S$  represents the area density.

## 4. Discussion

To further compare the structural difference of anthraquinone isomers, we systematically summarized the geometric characteristics, unit cell parameters and packing densities of self-assembled patterns of 1,8-A, 2,6-A, 1,4-A and 1,5-A ( $n = 15, 16$ ) molecules physisorbed at the 1-octanoic acid/HOPG interface, as shown in Table 1.

### 4.1 Role of $\pi$ -conjugated anthraquinone moieties and hydrogen bonds

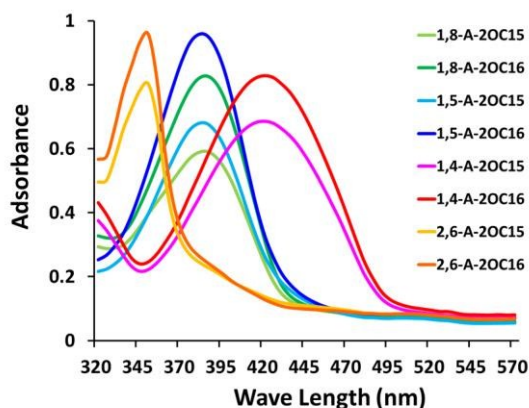
$\pi$ -Conjugated anthraquinone moieties play an important role in the process of forming orderly 2D self-assembled patterns because of its high electronic density. Besides, the orientation and dipole direction of two carbonyl groups in 9,10-position of the anthraquinone skeleton are reverse and thus lead to great structural symmetry. This symmetrical arrangement extinguishes the polarity of molecules, and as a result, anthraquinone derivatives show weak polarity. Therefore, the  $\pi$ -conjugated anthraquinone cores exert their role through van der Waals interaction between the anthraquinone core and the substrate,  $\pi$ - $\pi$  stacking and hydrogen bonding interactions. Moreover, due to its relatively strong, selective and directional nature, hydrogen bonds showed tremendous regulation in 2D crystal engineering. Tamaki *et al.* has reported the weak C=O $\cdots$ H-C hydrogen bonding formed between anthraquinone units, which was the dominant force on stabilizing the 2D self-assembled monolayers.<sup>54</sup> In structural isomers of 1,8-A, 2,6-A, 1,4-A and 1,5-A ( $n = 15, 16$ ), weak hydrogen bonds are

existent between anthraquinone moieties. This sort of hydrogen bond play an important role in the process of molecular recognition and then can give rise to well organized structures on surfaces.<sup>19</sup> In our study, hydrogen bonding interactions are powerful forces to make single molecules in a row to be orderly arranged, as shown in Fig. 2d, 2h, 3d, 3h, 5e, 7e, S3d (ESI $^+$ ) and S4d (ESI $^+$ ), illustrating the detailed information of C=O $\cdots$ H-C hydrogen bonds within different monolayers.

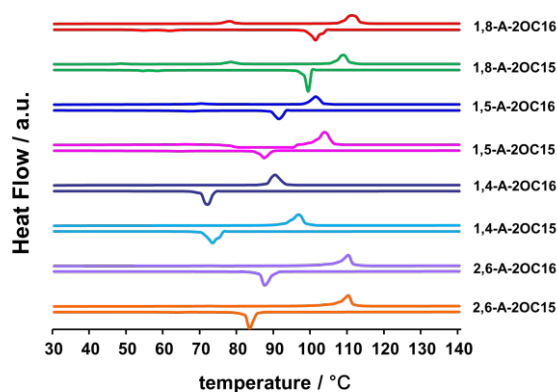
### 4.2 Alkyl chain position induced self-assembly diversity and property difference

Chemical structure is one of the dominant factors which exert direct influence on self-assembled monolayers on surface. Anthraquinone isomers are the target products obtained by changing the alkyl chain position, with the purpose of achieving diverse 2D nanostructures. In the case of cetyl substituted structural isomers, 1,8-A-2OC $_{16}$ , 2,6-A-2OC $_{16}$ , 1,4-A-2OC $_{16}$  and 1,5-A-2OC $_{16}$  adopted Z-like I (basic unit: dimer), Linear II (basic unit: trimer), Z-like II (basic unit: dimer) and Linear IV (basic unit: single molecule) structures, respectively. The calculated area densities for them are 1.33, 1.94, 2.44 and 3.08 nm $^2$  per molecule. It is obvious that the density order is 1,8-A-2OC $_{16}$  > 2,6-A-2OC $_{16}$  > 1,4-A-2OC $_{16}$  > 1,5-A-2OC $_{16}$ . However, in the case of pentadecyl substituted anthraquinone isomers, 1,8-A-2OC $_{15}$ , 2,6-A-2OC $_{15}$ , 1,4-A-2OC $_{15}$  and 1,5-A-2OC $_{15}$  adopted Linear I (basic unit: dimer), linear III (basic unit: single molecule), Z-like II (basic unit: dimer) and linear IV (basic unit: single molecule) structures, respectively. The calculated area densities for them are 1.78, 2.11, 2.52 and 2.97 nm $^2$  per molecule and the density order is 1,8-A-2OC $_{15}$  > 2,6-A-2OC $_{15}$  > 1,4-A-2OC $_{15}$  > 1,5-A-2OC $_{15}$ .





**Fig. 8** The UV absorption spectras of anthraquinone isomers in  $\text{CH}_2\text{Cl}_2$  solution at room temperature. Concentration:  $10^{-5}$  M ( $n = 16$ ) and  $10^{-6}$  M ( $n = 15$ ).



**Fig. 9** DSC thermograms of compounds 1,8-A, 2,6-A, 1,4-A and 1,5-A ( $n = 15, 16$ ) for the trace of heating (the above line) and cooling (the below line).

Anthraquinone isomers, have the same molecular formulas but adopt completely different assembly structures, have the same single-molecule area but show hugely different packing density which change in a large range. Therefore, we draw a conclusion that alkyl chain position can strongly regulate 2D self-assembled nanostructures.

As a step further, we conducted some performance testing. Different alkyl chain position can lead to entirely different chemical and physical properties. The most obvious indication of distinction between the anthraquinone isomers is color discrepancy. The four kinds of compounds were dissolved in  $\text{CH}_2\text{Cl}_2$ , and the solution color was compared at the concentration of  $10^{-2}$  M. As shown in Fig. S1 (ESI<sup>†</sup>), the immediate appearance of dark and light yellow color is characteristic of these structural isomers.

Fig. 8 shows the ultraviolet (UV) absorption spectrum of 1,8-A, 2,6-A, 1,4-A and 1,5-A ( $n = 15, 16$ ) compounds in  $\text{CH}_2\text{Cl}_2$  solution. They peak at 385, 350, 380 and 420 nm, respectively, as shown in Table S1 (ESI<sup>†</sup>), which is a summary for the maximum absorbance peaks of anthraquinone isomers. Concentration of these four kinds of isomers were  $10^{-5}$  M ( $n = 16$ ) and  $10^{-6}$  M ( $n = 15$ ). The characteristic peaks observed in Fig. 8 are assigned to  $\pi$ - $\pi^*$  electron transition<sup>55</sup>, and they are not related to the length of alkyl chains. Besides, the height of the absorbance peak is influenced by concentration of the solution. Then we adopted different concentration in order to avoid spectral line overlaps of compounds with the same substituent position but different chain length. We inferred that the observed spectral shift is correlated with the alkyl chain position, that is to say, structural isomers show different UV absorption properties.<sup>56,57</sup> For anthraquinone isomers, the adsorption peaks display gradual red-shift as the alkyl chain change from 2,6-position to 1,4-position, to 1,8-position, and then to 1,5-position.

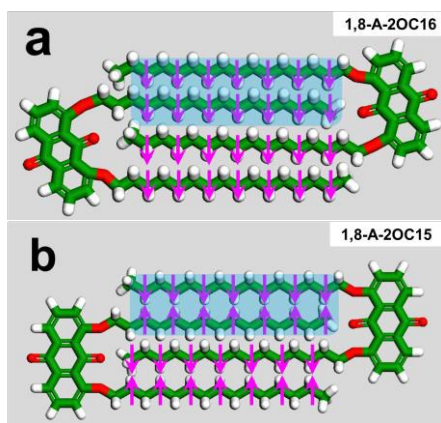
In addition, we investigated the phase transition behavior of these anthraquinone isomers. Differential scanning calorimetry (DSC) traces of 1,8-A, 2,6-A, 1,4-A and 1,5-A ( $n = 15, 16$ ) on heating are shown in Fig. 9. The property difference induced by alkyl chain position is remarkable, as indicated by the temperature in the horizontal ordinate, which is corresponded with the heat flow peak in the vertical coordinate. Clearing temperature (melting point)

variation tendency measured by the DSC experiments is 2,6-A-2OC<sub>16</sub> (117 °C) > 1,8-A-2OC<sub>16</sub> (112 °C) > 1,5-A-2OC<sub>16</sub> (102 °C) > 1,4-A-2OC<sub>16</sub> (91 °C) and 2,6-A-2OC<sub>15</sub> (111 °C) > 1,8-A-2OC<sub>15</sub> (109 °C) > 1,5-A-2OC<sub>15</sub> (104 °C) > 1,4-A-2OC<sub>15</sub> (97 °C), as also summarized in Table S2 (ESI<sup>†</sup>). This discrepancy of melting point is ascribed to different energy required to form uniform phase from the solid state.<sup>58</sup> Therefore, we conclude that these four kinds of anthraquinone isomers need quite different energy for self-assembling into ordered 2D formation, thus different kinds of structures are formed, which are stable both thermodynamically and kinetically.

### 4.3 Influence of odd/even number of carbon atoms in the alkyl chains on self-assembled nanostructures

Odd/even structural change in the alkyl chain has been identified as the possible origin of difference in the melting point and dynamic of monolayers<sup>59</sup>, thus it is a common phenomenon that odd/even number of the carbon atoms in the peripheral alkyl chains can greatly influence self-assembly structures. A large amount of papers have reported the dependence of molecular configurations on odd-even effect.<sup>42-46,60</sup> In this present work, the monolayers of 1,8-A and 2,6-A compounds are intimately related with the odd/even property of the side chains.

1,8-A-2OC<sub>16</sub> molecules gather together in a head-to-head fashion and then all of the acetabuliform dimers aggregate with each other, forming Z-like I stripes. Alkyl chains in adjacent stripes are interdigitated for close packing. But for 1,8-A-2OC<sub>15</sub>, molecules self-assembled into Linear I structure without Z-like stripes. Anthraquinone moieties are staggered in a head-to-head fashion, but alkyl chains in adjacent stripes are arranged in a tail-to-tail mode. It is well-known that the alkyl chains show great commensurability with the graphite surface and tend to extend along the direction of the main graphite axis so as to maximizing the adsorbate-substrate interactions.<sup>42,61</sup> We observed that alkyl chains of 1,8-A-2OC<sub>15</sub> in adjacent rows oriented at 120° angles or parallel to each other, as illustrated in Fig. 2f and S2 (ESI<sup>†</sup>), indicating the effect of substrate in the assembling process. Detailed information of these two structures is shown in Table 1. The non-interdigitated pentadecyl chains resulted in decreased area density for 1,8-A-2OC<sub>15</sub>, as the *S* value of 1.78 nm<sup>2</sup> denoted, by comparing with 1.33 nm<sup>2</sup> for 1,8-A-2OC<sub>16</sub>. A question arises why 1,8-A-2OC<sub>16</sub>

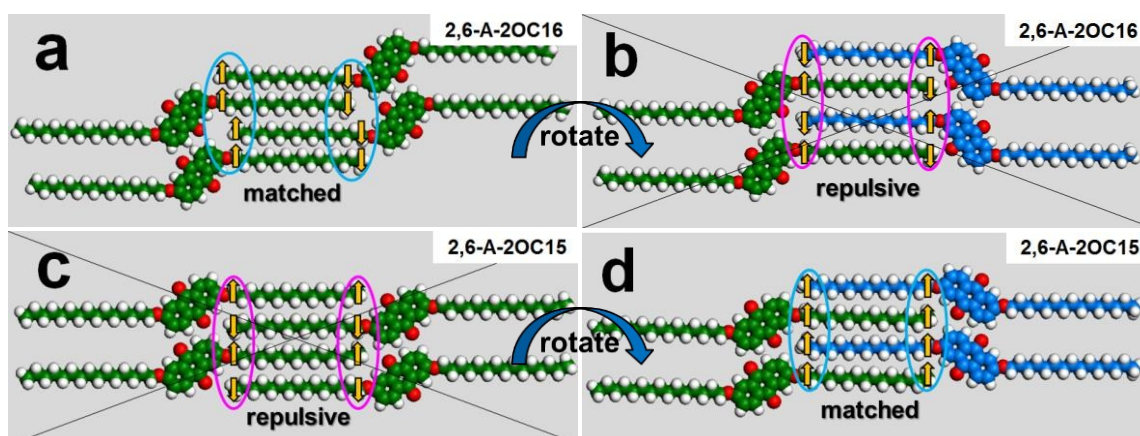


**Fig. 10** Stick model of 1,8-A-2OC<sub>16</sub> and 1,8-A-2OC<sub>15</sub>. (a) The actual model based on STM results. (b) The assumed model in which alkyl chains are interdigitated. The direction of carbon atoms is denoted by pink arrows. The repulsive and non-repulsive regions are marked by blue rectangles for ease of comparison.

self-assembled into closed structures with the alkyl chains interdigitated with each other, but side chains of 1,8-A-2OC<sub>15</sub> were arranged in a tail-to-tail fashion. Same STM results from experiments with solution concentration varying from 5% saturation ( $4.84 \times 10^{-4}$  M) to 100% saturation ( $9.68 \times 10^{-3}$  M) indicate the phenomenon of non-interdigitated alkyl chains was caused by odd number of carbon atoms in the side chains instead of the low concentration. Fig. 10 is the stick model of 1,8-A-2OC<sub>16</sub> and 1,8-A-2OC<sub>15</sub>. The long chains are tiled on the substrate, and carbon atoms are connected in an up-down-up-down (zigzag) way. The angle between the alkyl chain and the macroaxis of the anthraquinone is corresponded with the STM results shown in Fig. 2b and 2f. For molecule of 1,8-A-2OC<sub>16</sub>, carbon atoms in neighboring chains are orienting to the same direction, as shown in Fig. 10a by pink arrows, and the steric repulsion is reduced. Alkyl chains of 1,8-A-2OC<sub>15</sub> molecules are assumed to be staggered in an interdigitated fashion, as shown in Fig. 10b. However, in this hypothetical case, no matter

how molecules are moved along the direction of the chains, part of the carbon atoms in neighboring chains are orienting into a head-to-head fashion, as the head-to-head arrows indicated. As a result, steric repulsion is too strong to be able to stabilize the adsorbates and consequently, interdigitated alkyl chains of 1,8-A-2OC<sub>15</sub> are nonexistent.

2,6-A-2OC<sub>16</sub> molecules adopted Linear II structure. It can be clearly seen that the basic unit of the monolayer is a number of trimers, which are indicated by pink rectangles in Fig. 3b and 3c. Trimers in a row are discontinuous, showing orderly dislocation along the direction of the alkyl chains and molecules in neighboring rows are parallel to each other. Nevertheless, anthraquinone units of 2,6-A-2OC<sub>15</sub> molecules in neighboring rows are not parallel, forming a V-like fashion, named as Linear III structures. Both of these two structures are close packing, without uncovered HOPG surface, though the calculated area density for 2,6-A-2OC<sub>16</sub> ( $S = 1.94$  nm<sup>2</sup> per molecule) is slightly higher than that for 2,6-A-2OC<sub>15</sub> ( $S = 2.11$  nm<sup>2</sup> per molecule). Fig. 11a and 11d are the space-filling sphere figures which display the matched end methyls with methylene groups within the interdigitated side chains. Adjacent alkyl chains tend to be arranged with their end methyls orienting to the direction of the methylenes which are connected with the ether groups. This is necessary for avoiding or decreasing steric repulsion. 2,6-A-2OC<sub>16</sub> molecules are staggered with the anthraquinones parallel to each other, but 2,6-A-2OC<sub>15</sub> molecules adopted a V-like fashion. Careful analysis indicates that the nonparallel rows for 2,6-A-2OC<sub>15</sub> are needed for changing the direction of the end methyl and then get well-matched alkyl chains. For the purpose of exploring why anthraquinone in these two molecules are arranged in different ways, we put forward two hypothetical cases, as shown in Fig. 11b and 11c. The carbon atom skeletons of the rotated molecules are denoted in blue for ease of distinguishing. The yellow arrows indicate the direction of the end methyls and the methylenes which are connected with the ether groups. Arrows in the blue ovals (Fig. 11a and 11d) are orienting to the same direction, leading to matched alkyl chains. But in the pink ovals (Fig. 11b and 11c), neighboring arrows are in a head-to-head or tail-to-tail way.



**Fig. 11** Space-filling spheres figure representation of the matched end methyls with methylene groups within the interdigitated side chains. The orange arrows indicate the direction of the end carbon atoms. Blue and pink ovals represent the matched and repulsive carbon atoms, respectively. (a and c) Models for 2,6-A-2OC<sub>16</sub> and 2,6-A-2OC<sub>15</sub>, with the anthraquinones in neighboring rows arranged parallel to each other. (b and d) Models for 2,6-A-2OC<sub>16</sub> and 2,6-A-2OC<sub>15</sub>, with the anthraquinones in neighboring rows arranged in a V-like fashion, which are the result of rotating from (a) and (c).



It is easy to judge that steric repulsion of Fig. 11a is smaller than that of Fig. 11b, and steric repulsion of Fig. 11d is smaller than that of Fig. 11c. Therefore, the assumed cases shown in Fig. 11b and 11c are unreasonable, and molecule rotation for 2,6-A-2OC<sub>15</sub> is needed.

However, 1,4-A and 1,5-A showed no structural difference when the alkyl chain length ( $n = 15, 16$ ) is taken into consideration. Both of 1,4-A-2OC<sub>16</sub> and 1,4-A-2OC<sub>15</sub> adopted Z-like II structure. The detailed differences between them are unit cell parameters, as summarized in Table 1. Area density for the former is 2.44 nm<sup>2</sup> per molecule and 2.52 nm<sup>2</sup> per molecule for the latter. 1,4-A-2OC<sub>16</sub> molecule is larger by one methylene in the side chain than 1,4-A-2OC<sub>15</sub>, while area for single molecule for 1,4-A-2OC<sub>16</sub> is smaller than that for 1,4-A-2OC<sub>15</sub>. Thus, we confirm that the Z-like II structure for 1,4-A-2OC<sub>16</sub> is denser than that for 1,4-A-2OC<sub>15</sub>. 1,5-A-2OC<sub>16</sub> and 1,5-A-2OC<sub>15</sub> self-assembled into the same linear IV structure. 1,5-A-2OC<sub>16</sub> molecule is larger by one methylene in the side chain than 1,4-A-2OC<sub>15</sub>, and area density for single molecule for the former ( $S = 3.08$  nm<sup>2</sup> per molecule) is slightly larger than that for the latter ( $S = 2.97$  nm<sup>2</sup> per molecule). Then we infer that the degree of close packing for 1,5-A-2OC<sub>16</sub> and 1,5-A-2OC<sub>15</sub> is nearly the same. The non-emergence of odd/even effect for 1,4-A and 1,5-A can be regarded as an indication that the driving force for them to self-assemble into ordered monolayers are van der Waals interactions between molecule–molecule, molecule–substrate, and hydrogen bonds among anthraquinones moieties, and they are strong enough to stabilize the molecules, without taking well-matched alkyl chains into consideration.

## 5. Conclusion

Structural isomers of anthraquinone derivatives 1,8-A, 2,6-A, 1,4-A and 1,5-A ( $n = 15, 16$ ) were synthesized and tested *via* STM for the sake of exploring how alkyl chain position and odd/even property can influence the self-assembled patterns on liquid/solid surface of HOPG. Weak hydrogen bonds, alkyl chain interdigitation,  $\pi$ – $\pi$  stacking and adsorbate–substrate interactions are the main forces which dominated anthraquinone derivatives to stagger into ordered and close packing. 1,8-A, 2,6-A, 1,4-A and 1,5-A with side chains of  $n = 16$  adopted Z-like I, Linear II, Z-like II and Linear IV phases, respectively. Structural differences were induced by change of the substituent position. Comparing with 1,8-A-2OC<sub>16</sub> and 2,6-A-2OC<sub>16</sub>, 1,8-A-2OC<sub>15</sub> and 2,6-A-2OC<sub>15</sub> self-assembled into Linear I and Linear III arrangements, indicating that odd/even number of carbon atoms in the alkyl chain can influence the process of self-assembly. However, 1,4-A and 1,5-A showed no odd–even effect induced structural difference, and then we make a conclusion that the driving forces for 1,4-A and 1,5-A molecules to be orderly arranged on HOPG surface were hydrogen bonding and molecule–substrate interactions. Moreover, chirality was observed for achiral molecules of 2,6-A-2OC<sub>16</sub>, and the left-handed and right-handed networks are regardless of priorities. Much is to be learned and explored on regulating the process of self-assembly for anthraquinone isomers.

## Acknowledgments

Financial supports from the National Program on Key Basic Research Project (2012CB932900), the National Natural Science Foundation of China (21573077, 51373055, 21403072), the China Postdoctoral Science Foundation (2014M552189), and the Fundamental Research Funds for the Central Universities (SCUT) are gratefully acknowledged.

## References

- 1 K. S. Mali, K. Lava, K. Binnemans and S. De Feyter, *Chem. Eur. J.*, 2010, **16**, 14447–14458.
- 2 J. M. Lehn, *Proc. Natl. Acad. Sci. USA*, 2002, **99**, 4763–4768.
- 3 G. M. Whitesides and M. Boncheva, *Proc. Natl. Acad. Sci. USA*, 2002, **99**, 4769–4774.
- 4 C. Joachim, J. K. Gimzewski and A. Aviram, *Nature*, 2000, **408**, 541–548.
- 5 A. Nitzan and M. A. Ratner, *Science*, 2003, **300**, 1384–1389.
- 6 J. V. Barth, J. Weckesser, C. Cai, P. Günter, L. Bürgi, O. Jeandupeux and K. Kern, *Angew. Chem.*, 2000, **112**, 1285–1288.
- 7 J. V. Barth, J. Weckesser, C. Z. Cai, P. Gunter, L. Burgi, O. Jeandupeux and K. Kern, *Angew. Chem. Int. Ed.*, 2000, **39**, 1230–1234.
- 8 K. W. Hipps, L. Scudiero, D. E. Barlow and M. P. Cooke, *J. Am. Chem. Soc.*, 2002, **124**, 2126–2127.
- 9 S. De Feyter, M. M. S. A. Mottaleb, N. Schuurmans, B. J. V. Verkuijl, J. H. V. Esch, B. L. Feringa and F. C. De Schryver, *Chem. Eur. J.*, 2004, **10**, 1124–1132.
- 10 D. G. Choi, S. Kim, E. Lee and S. M. Yang, *J. Am. Chem. Soc.*, 2005, **127**, 1636–1637.
- 11 M. Lackinger, S. Griessl, W. M. Heckl, M. Hietschold and G. W. Flynn, *Langmuir*, 2005, **21**, 4984–4988.
- 12 L. Xu, X. R. Miao, L. H. Cui, P. Liu, K. Miao, X. F. Chen and W. L. Deng, *J. Phys. Chem. C*, 2015, **119**, 17920–17929.
- 13 M. Ruben, *Angew. Chem.*, 2005, **117**, 1620–1623.
- 14 J. A. A.W. Elemans and S. De Feyter, *Soft Matter*, 2009, **5**, 721–735.
- 15 A. G. Phillips, L. M. A. Perdigo, P. H. Beton and N. R. Champness, *Chem. Commun.*, 2010, **46**, 2775–2777.
- 16 S. Chiang, *Chem. Rev.*, 1997, **97**, 1083–1096.
- 17 S. De Feyter and F. C. De Schryver, *J. Phys. Chem. B*, 2005, **109**, 4290–4302.
- 18 K. Tahara, K. Inukai, N. Hara, C. A. Johnson II, M. M. Haley and Y. Tobe, *Chem. Eur. J.*, 2010, **16**, 8319–8328.
- 19 L. Kampschulte, M. Lackinger, A. K. Maier, R. S. K. Kishore, S. Griessl, M. Schmittel and W. M. Heckl, *J. Phys. Chem. B*, 2006, **110**, 10829–10836.
- 20 L. Kampschulte, T. L. Werblowsky, R. S. K. Kishore, M. Schmittel, W. M. Heckl and M. Lackinger, *J. Am. Chem. Soc.*, 2008, **130**, 8502–8507.
- 21 Z. Mu, L. Shu, H. Fuchs, M. Mayor and L. Chi, *J. Am. Chem. Soc.*, 2008, **130**, 10840–10841.
- 22 M. A. Lingenfelder, H. Spillmann, A. Dmitriev, S. Stepanow, N. Lin, J. V. Barth and K. Kern, *Chem. Eur. J.*, 2004, **10**, 1913–1919.
- 23 S. Stepanow, N. Lin, D. Payer, U. Schlickum, F. Klappenberger, G. Zoppellaro, M. Ruben, H. Brune, J. V. Barth and K. Kern, *Angew. Chem.*, 2007, **119**, 724–727.

- 24 M. Surin, P. Samori, A. Jouaiti, N. Kyritsakas and M. W. Hosseini, *Angew. Chem.*, 2007, **119**, 249–253.
- 25 T. Yokoyama, S. Yokoyama, T. Kamikado, Y. Okuno and S. Mashiko, *Nature*, 2001, **413**, 619–621.
- 26 M. de Wild, S. Berner, H. Suzuki, H. Yanagi, D. Schlettwein, S. Ivan, A. Baratoff, H. J. Guentherodt and T. A. Jung, *ChemPhysChem*, 2002, **3**, 881–885.
- 27 Y. Wei, W. Tong, C. Wise, X. Wei, K. Armbrust and M. Zimmt, *J. Am. Chem. Soc.*, 2006, **128**, 13362–13363.
- 28 Y. Wei, W. Tong and M. B. Zimmt, *J. Am. Chem. Soc.*, 2008, **130**, 3399–3405.
- 29 X. Qiu, C. Wang, Q. Zeng, B. Xu, S. Yin, H. Wang, S. Xu and C. Bai, *J. Am. Chem. Soc.*, 2000, **122**, 5550–5556.
- 30 Z. Y. Yang, H. M. Zhang, C. J. Yan, S. S. Li, H. J. Yan, W. G. Song and L. J. Wan, *Proc. Natl. Acad. Sci. USA*, 2007, **104**, 3707–3712.
- 31 R. Gutzler, T. Sirtl, J. F. Dienstmaier, K. Mahata, W. M. Heckl, M. Schmittel and M. Lackinger, *J. Am. Chem. Soc.*, 2010, **132**, 5084–5090.
- 32 C. Marie, F. Silly, L. Torteche, K. Müllen and D. Fichou, *ACS Nano.*, 2010, **4**, 1288–1292.
- 33 D. Rohde, C. J. Yan, H. J. Yan and L. J. Wan, *Angew. Chem. Int. Ed.*, 2006, **45**, 3996–4000.
- 34 C. J. Li, Q. D. Zeng, Y. H. Liu, L. J. Wan, C. Wang, C. R. Wang and C. L. Bai, *ChemPhysChem*, 2003, **4**, 857–859.
- 35 S. Lei, K. Tahara, F. C. De Schryver, M. Van der Auweraer, Y. Tobe and S. De Feyter, *Angew. Chem.*, 2008, **120**, 3006–3010.
- 36 C. A. Palma, M. Bonini, A. Llanes-Pallas, T. Breiner, M. Prato, D. Bonifazi and P. Samori, *Chem. Commun.*, 2008, **42**, 5289–5291.
- 37 C. A. Palma, J. Bjork, M. Bonini, M. S. Dyer, A. L. Pallas, D. Bonifazi, M. Persson and P. Samori, *J. Am. Chem. Soc.*, 2009, **131**, 13062–13071.
- 38 K. Tahara, S. Okuhata, J. Adisojoso, S. Lei, T. Fujita, S. De Feyter and Y. Tobe, *J. Am. Chem. Soc.*, 2009, **131**, 17583–17590.
- 39 L. Piot, A. Marchenko, J. Wu, K. Müllen and D. Fichou, *J. Am. Chem. Soc.*, 2005, **127**, 16245–16250.
- 40 Y. Kikkawa, E. Koyama, S. Tsuzuki, K. Fujiwara and M. Kanesato, *Langmuir*, 2010, **26**, 3376–3381.
- 41 C. Fu, F. Rosei and D. F. Perepichka, *ACS Nano*, 2012, **6**, 7973–7980.
- 42 I. De Cat, C. Gobbo, B. Van Averbek, R. Lazzaroni, S. De Feyter and J. V. Esch, *J. Am. Chem. Soc.*, 2011, **133**, 20942–20950.
- 43 H. Fang, L. C. Giancarlo and G. W. Flynn, *J. Phys. Chem. B*, 1998, **102**, 7421–7424.
- 44 Y. Kikkawa, E. Koyama, S. Tsuzuki, K. Fujiwara, K. Miyake, H. Tokuhisa and M. Kanesato, *Chem. Commun.*, 2007, **13**, 1343–1345.
- 45 F. Tao and S. L. Bernasek, *Chem. Rev.*, 2007, **107**, 1408–1453.
- 46 F. Tao, J. Goswami and S. L. Bernasek, *J. Phys. Chem. B*, 2006, **110**, 4199–4206.
- 47 A. E. Murschell, W. H. Kan, V. Thangadurai and T. C. Sutherland, *Phys. Chem. Chem. Phys.*, 2012, **14**, 4626–4634.
- 48 M. Pokrifchak, T. Turner, I. Pilgrim, M. R. Johnston and K. W. Hipps, *J. Phys. Chem. C*, 2007, **111**, 7735–7740.
- 49 L. Xu, X. R. Miao, L. H. Cui, P. Liu, X. F. Chen and W. L. Deng, *Nanoscale*, 2015, **7**, 11734–11745.
- 50 T. Chen, W. H. Yang, D. Wang and L. J. Wan, *Nat. Commun.*, 2013, **4**, 1389–1397.
- 51 F. Masini, N. Kalashnyk, M. M. Knudsen, J. R. Cramer, E. Lægsgaard, F. Besenbacher, K. V. Gothelf and T. R. Linderoth, *J. Am. Chem. Soc.*, 2011, **133**, 13910–13913.
- 52 K. Tahara, H. Yamaga, E. Ghijsens, K. Inukai, J. Adisojoso, M. O. Blunt, S. De Feyter and Y. Tobe, *Nat. Chem.*, 2011, **3**, 714–719.
- 53 M. Parschau, S. Romer and K. H. Ernst, *J. Am. Chem. Soc.*, 2004, **126**, 15398–15399.
- 54 T. Yoshinori, M. Kosuke and M. Kazuo, *Bull. Chem. Soc. Jpn.*, 2013, **86**, 354–362.
- 55 L. H. Cui, X. R. Miao, L. Xu, Y. Hu and W. L. Deng, *Phys. Chem. Chem. Phys.*, 2015, **17**, 3627–3636.
- 56 H. Fan, J. Smuts, L. Bai, P. Walsh, D. W. Armstrong and K. A. Schug, *Food Chem.*, 2016, **194**, 265–271.
- 57 L. Jin and P. Zhang, *Chem. Eng. J.*, 2015, **280**, 241–247.
- 58 J. Y. Wang, J. Yan, L. Ding, Y. Ma and J. Pei, *Adv. Funct. Mater.*, 2009, **19**, 1746–1752.
- 59 G. M. Florio, T. L. Werblowsky, B. Ilan, T. Müller, B. J. Berne and G. W. Flynn, *J. Phys. Chem. C*, 2008, **112**, 18067–18075.
- 60 L. Xu, X. R. Miao, B. Zha, K. Miao and W. L. Deng, *J. Phys. Chem. C*, 2013, **117**, 12707–12714.
- 61 J. P. Rabe and S. Buchholz, *Science*, 1991, **253**, 424–427.